Computers and Structures 320 (2026) 108049

Contents lists available at ScienceDirect

Computers and Structures

journal homepage: www.elsevier.com/locate/compstruc

The overlapping spectral element method

Pooya Zakian [a,b], Klaus-Jürgen Bathe [c,*]

[a] Department of Civil Engineering, Faculty of Engineering, Arak University, Arak, Iran
[b] Faculty of Civil and Environmental Engineering, Tarbiat Modares University, Tehran, Iran
[c] Department of Mechanical Engineering, Massachusetts Institute of Technology, Cambridge, MA 02139, United States

ARTICLE INFO

Keywords:
Overlapping spectral element method
Explicit/implicit Bathe time integration
Lumped mass
CAD geometry
Structural dynamics
Wave propagation

ABSTRACT

In this study, we develop a novel computational framework called Overlapping Spectral Element Method (OSEM). The OSEM is based on the overlapping finite element method and spectral element method with higher-order interpolation functions, which can be effective for the analysis of structural dynamics and wave propagation problems. In this method, there are three types of spectral elements: regular, coupling, and overlapping. The mass matrices of overlapping and coupling elements are not diagonal, whereas the mass matrices of regular spectral elements are inherently diagonal. Hence, using the elements employed in the mesh, an explicit–implicit or implicit time integration method can be utilized for the time integration. The OSEM includes the advantages of both overlapping finite element and spectral element methods to provide higher accuracy and less element geometric distortion sensitivity than the traditional spectral element method in modeling complex domains. Finally, we demonstrate the merits of using the proposed solution procedure in comparison to using the traditional spectral element method in the solution of several numerical examples.

1. Introduction

Almost any kind of structural/mechanical system may be affected by at least one form of dynamic loading (e.g., earthquake, wind, ocean wave, and impulse) during its lifetime, and therefore dynamic analyses of the system are inevitable. As few examples, we mention the time-history dynamic analysis of structures subjected to seismic loading, the effects of hydrodynamic pressures on dams, and the analysis of fault rupture dynamics. In particular, the solution of wave propagations is a challenging problem in various engineering disciplines as in computational earthquake engineering [1–3] and structural health monitoring [4]. Since only simple cases of wave propagations have analytical solutions, numerical solutions are sought and much research effort has been expended in using the finite element method for wave propagations [5]. These research efforts have had only limited success because unacceptable dispersion and dissipation errors arise when considering wave propagations in a geometrically complex domain. The fundamental reason is that the waves travel in possibly any direction, and at different speeds, through a mesh of elements with different "characteristic element lengths". These difficulties using the traditional finite element method are even present when the mesh for a two- or three-dimensional domain is regular containing only non-distorted elements.

The problem of too large dispersion and dissipation errors have been largely overcome in the *overlapping finite element method* enriched with harmonic functions [6–9]. The reason is that the overlapping finite elements are largely distortion-insensitive [8] and when enriched with harmonic functions contain the basic interpolations to represent wave propagations [7,9].

Another solution scheme that can be used in the solution of wave propagations is the spectral element method, also known as spectral finite element method [10–13]. However, this solution method also results in dispersion and dissipation errors, albeit not as large errors as in the traditional finite element method using low-order elements. The reason is that high-order elements are used that show less sensitivity to element distortions and with special integration schemes that automatically result in a diagonal mass matrix—although interpolations are employed that correspond to the *Ansatz* of a consistent mass matrix. Hence an explicit time integration scheme like the Noh-Bathe method can directly be used. Moreover, the distribution of nodes in the spectral element is nonuniform with nodes placed near the element corners which prevents the Runge phenomenon—that is, it prevents large oscillations of polynomial values near the corners if equally-spaced nodes were used [4]. A comprehensive dispersion analysis of this explicit time integration scheme with the spectral element method has been reported

* Corresponding author.
E-mail address: kjb@mit.edu (K.J. Bathe).

https://doi.org/10.1016/j.compstruc.2025.108049
Received 5 September 2025; Accepted 17 November 2025
Available online 25 November 2025

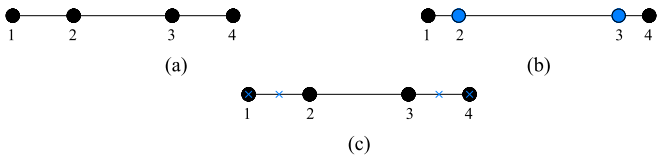

Fig. 1. Steps of constructing a one-dimensional overlapping spectral element: (a) spectral element of order 3, (b) fictitious spectral element of order 3, and (c) overlapping spectral element of order 3; the black nodes are the original nodes, whereas the blue nodes are the additional fictitious nodes. (For interpretation of the references to colour in this figure legend, the reader is referred to the web version of this article.)

in Ref. [10] where some mathematical formulations were also derived to distinguish the dispersion errors due to the spatial discretization from those caused by the time discretization. Also, an analysis to establish a suitable Courant–Friedrichs–Lewy (CFL) number was carried out.

The overlapping finite element method was established using the method of finite spheres (which naturally overlap). In this meshless method, the Shepard functions are utilized for the spatial interpolations resulting in a large integration effort, because these functions are rational functions [14]. Indeed, all meshless methods that are based on interpolations without the use of stability factors require a large computational effort for the spatial integrations which significantly limits their use in practice. In contrast to the method of finite spheres, the overlapping elements use neither rational functions nor their derivatives in the formation of element matrices [6], thereby significantly reducing the computational effort required for the numerical integration. In addition, a mesh of overlapping elements is constructed like a mesh of low-order finite elements, for example, for 3-node overlapping finite elements like for 3-node triangular traditional finite elements. Hence the element connectivity of an overlapping element is identical to that of a traditional low-order finite element, and the overlapping element can be directly embedded into a mesh of traditional low-order

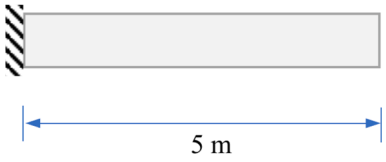

Fig. 3. A clamped rod used for the analysis of vibration frequencies.

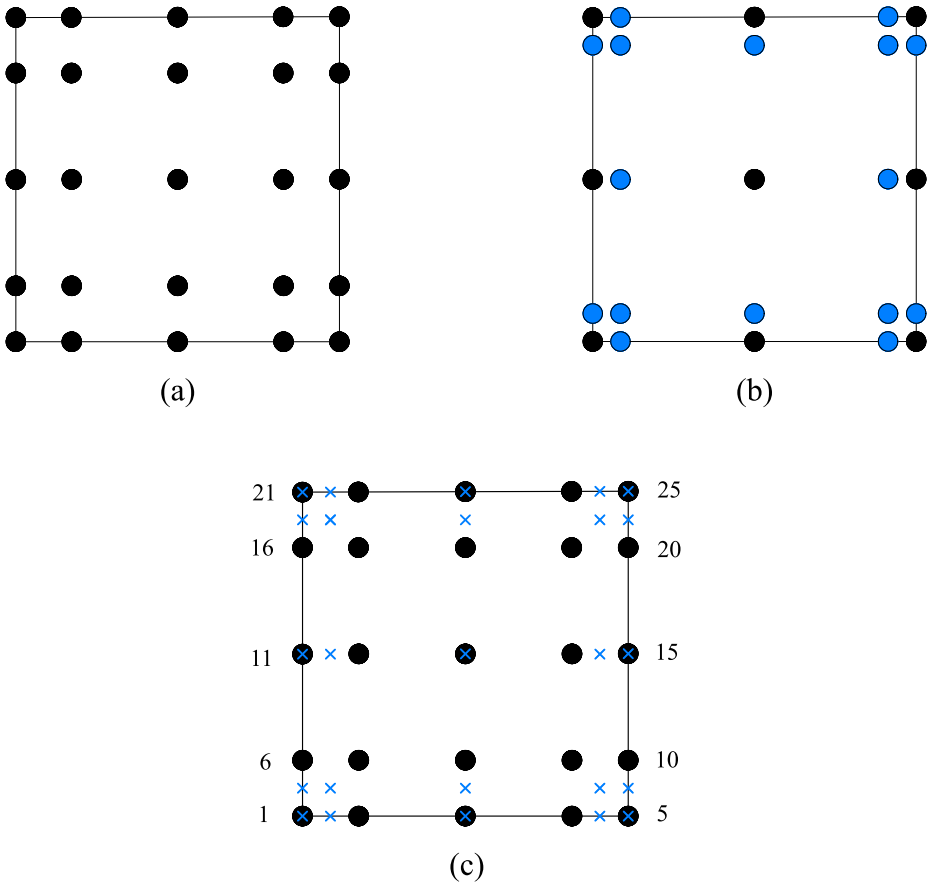

Fig. 2. Construction steps of a two-dimensional overlapping spectral element: (a) spectral element of order 4, (b) fictitious spectral element of order 4, and (c) overlapping spectral element of order 4; the black nodes are the original nodes, whereas the blue nodes are the additional fictitious nodes. (For interpretation of the references to colour in this figure legend, the reader is referred to the web version of this article.)

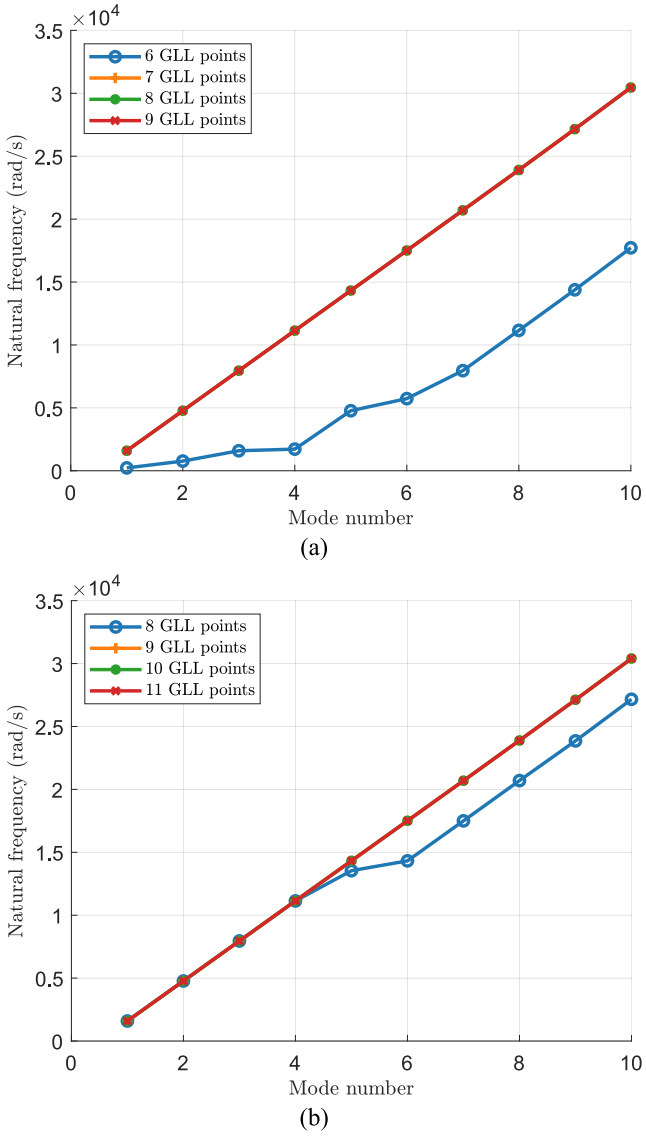

Fig. 4. Computed eigenvalues using various numbers of GLL points: (a) overlapping spectral element of order 3, and (b) overlapping spectral element of order 4.

finite elements. It follows that a mesh generator for the traditional finite element method of low-order elements can be directly used in the overlapping finite element method. However, other than the low-order traditional elements, the overlapping elements can represent high-order variations of solutions and preserve polynomial completeness in a distorted mesh. The elements are largely distortion-insensitive [8].

The overlapping finite element method incorporates the concept of *automatic meshing with overlapping and regular elements* (AMORE) [6]. In the AMORE concept, a computational domain is filled mostly with *regular* elements (also called *traditional* or *undistorted* elements), whereas the geometrically complicated regions of the computational domain are filled with *overlapping* elements that can be highly distorted without losing predictive capability. The elements connecting the overlapping elements to the traditional elements are the *coupling* elements. While the first overlapping elements used values of the Shepard functions at specific locations to establish the polynomial interpolations, an improved overlapping element formulation was presented recently [14]. In this formulation, values of Shepard functions are no longer used for constructing the displacement interpolations, and the formulation is very general for two- and three-dimensional elements and solutions.

The overlapping finite element method has successfully been applied to solve structural dynamics and wave propagation problems. Using harmonic basis functions in addition to the low-order polynomial interpolations, very accurate solutions are obtained even when distorted elements are employed [7–9]. Naturally, the harmonic basis functions increase the total number of degrees of freedom leading to a larger computational cost of solution. The cost is further increased when the method is used with the consistent mass matrix and implicit time integration requiring the initial factorization of the coefficient matrix and for each time step a forward reduction and back-substitution [5,15]. The implicit time integration method can usually be employed with a larger time-step size than an explicit time integration method, hence uses less time steps, but the computational effort per time step is much larger than when using an explicit time integration scheme.

In this paper, we focus on the development of the *overlapping spectral element method*. For the formulation of this method, we consider the higher-order interpolation functions used in the spectral element method established by Lagrange polynomials with Lobatto collocation points and Gauss–Lobatto–Legendre (GLL) quadrature. The formulation does not use any additional basis functions (like harmonic functions) because the interpolation functions of overlapping spectral element are sufficient to reach a desirable accuracy for dynamic and wave

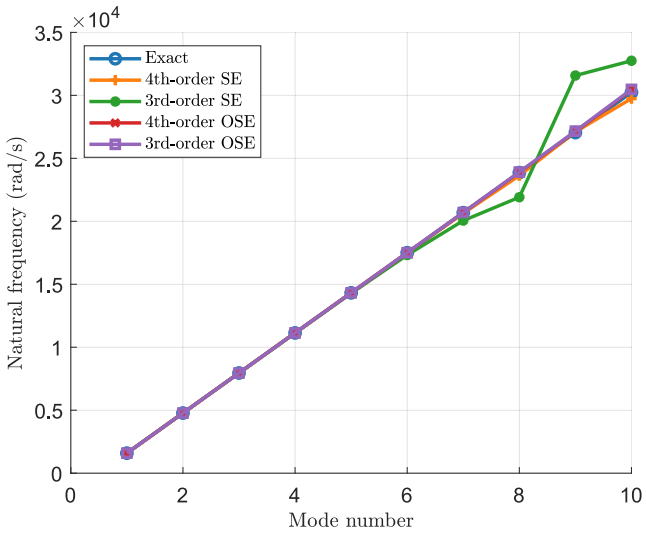

Fig. 5. Comparison of eigenvalues computed using analytical method, spectral elements of orders 3 and 4, overlapping spectral element of orders 3 and 4; considering appropriate numbers of GLL points for the numerical solutions.

propagation analyses. Further, we present a simplified formulation of the overlapping spectral element method for ease of computer implementation and will show that this method gives desirable solution accuracy and outperforms the spectral element method suffering from element distortion-sensitivity.

The presentation is organized as follows. Section 2 introduces the overlapping spectral element method with the formulations for solutions in elastodynamics. Section 3 presents some insights into the interpolation functions of one- and two-dimensional overlapping spectral elements. Then in Section 4, some numerical examples of structural dynamics and wave propagation are provided. Finally, Section 5 gives the concluding remarks.

2. Formulation of overlapping spectral element method

A mesh of the overlapping spectral element method using the AMORE concept contains three types of elements: regular spectral elements, overlapping spectral elements, and coupling spectral elements for which we develop the formulation in this section. Of course, we may use only the overlapping spectral elements in a mesh to achieve a desirable solution accuracy.

In general, the governing equation of a problem in elastodynamics is in matrix form, neglecting physical damping,

$$\mathbf{M}\ddot{\mathbf{U}} + \mathbf{K}\mathbf{U} = \mathbf{F} \tag{1}$$

where $\mathbf{M}$, $\mathbf{K}$ and $\mathbf{F}$ denote the mass matrix, stiffness matrix, and force vector, respectively. Also, $\ddot{\mathbf{U}}$ and $\mathbf{U}$ list the nodal accelerations and displacements, respectively. In addition, the initial conditions at time 0 need to be specified.

2.1. Regular spectral element

A *regular* spectral element refers to the standard element used in the spectral element method, containing only traditional degrees of freedom. The interpolation functions of a spectral element are given by the Lagrange interpolation functions using the Lobatto collocation points. Also, the numerical integration used in the formation of the element matrices is the GLL quadrature. Since the abscissa of the GLL and the zeros of the interpolation functions are identical, the mass

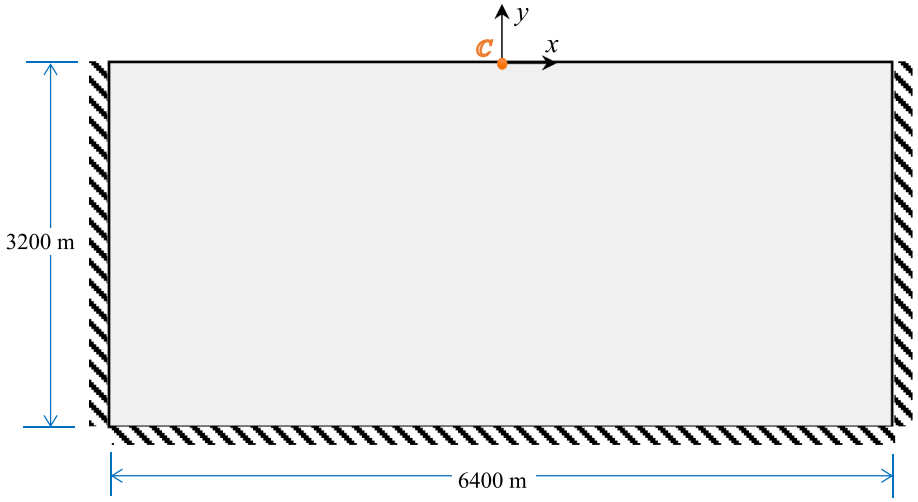

Fig. 6. Computational domain of Lamb's problem defined for wave propagation within semi-infinite elastic medium, where the excitation force is applied at point C and two receivers are located at (−640 m, 0) and (−1280 m, 0).

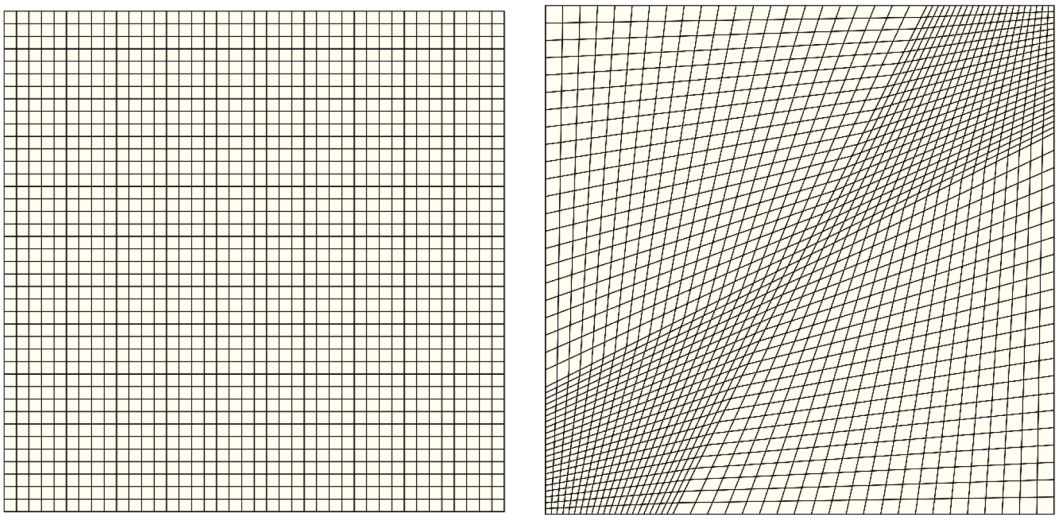

(a) (b)

Fig. 7. Meshes used for the uniform semi-infinite medium: (a) uniform mesh of 40 × 40 elements, and (b) distorted mesh of 1936 elements.

matrix is diagonal.

In the isoparametric formulation of a one-dimensional spectral element of order n, the GLL points are given by the roots of the following equation:

$$(1-r^2)P'_{n-1}(r)=0 \tag{2}$$

where $P_n(r)$ is the Legendre polynomial of degree n, that is

$$P_n(r)=\frac{1}{2^n n!}\frac{\mathrm{d}^n}{\mathrm{d}r^n}(r^2-1)^n \tag{3}$$

interpolations by multiplications.

For the mth spectral element, the displacement vector is obtained by

$$\mathbf{U}^{(m)}=\mathbf{H}^{(m)}\mathbf{a}^{(m)} \tag{4}$$

where $\mathbf{a}^{(m)}$ lists the unknowns constituting the nodal displacements, and $\mathbf{H}^{(m)}$ is the matrix of interpolation functions. As an example, the 3rd-order interpolation functions of a quadrilateral spectral element are [16,17]

$$\begin{aligned}
h_1&=\frac{1}{64}(5r^2-1)(5s^2-1)(r-1)(s-1), & h_2&=-\frac{\sqrt{5}}{64}(5r-\sqrt{5})(5s^2-1)(r^2-1)(s-1),\\
h_3&=\frac{\sqrt{5}}{64}(5r+\sqrt{5})(5s^2-1)(r^2-1)(s-1), & h_4&=-\frac{1}{64}(5r^2-1)(5s^2-1)(r+1)(s-1),\\
h_5&=-\frac{\sqrt{5}}{64}(5r^2-1)(5s-\sqrt{5})(r-1)(s^2-1), & h_6&=\frac{5}{64}(5r-\sqrt{5})(5s-\sqrt{5})(r^2-1)(s^2-1),\\
h_7&=-\frac{5}{64}(5r+\sqrt{5})(5s-\sqrt{5})(r^2-1)(s^2-1), & h_8&=\frac{\sqrt{5}}{64}(5r^2-1)(5s-\sqrt{5})(r+1)(s^2-1),\\
h_9&=\frac{\sqrt{5}}{64}(5r^2-1)(5s+\sqrt{5})(r-1)(s^2-1), & h_{10}&=-\frac{5}{64}(5r-\sqrt{5})(5s+\sqrt{5})(r^2-1)(s^2-1),\\
h_{11}&=\frac{5}{64}(5r+\sqrt{5})(5s+\sqrt{5})(r^2-1)(s^2-1), & h_{12}&=-\frac{\sqrt{5}}{64}(5r^2-1)(5s+\sqrt{5})(r+1)(s^2-1),\\
h_{13}&=-\frac{1}{64}(5r^2-1)(5s^2-1)(r-1)(s+1), & h_{14}&=\frac{\sqrt{5}}{64}(5r-\sqrt{5})(5s^2-\sqrt{5})(r^2-1)(s+1),\\
h_{15}&=-\frac{\sqrt{5}}{64}(5r+\sqrt{5})(5s^2-1)(r^2-1)(s+1), & h_{16}&=\frac{1}{64}(5r^2-1)(5s^2-1)(r+1)(s+1).
\end{aligned} \tag{5}$$

This is why this variant of spectral element is also known as a Legendre-based spectral element. After determining the GLL points, they are used in the Lagrange interpolation to construct the interpolation functions of a spectral element. As in the formulation of the traditional finite elements, we obtain the interpolation functions of two- and three-dimensional spectral elements from the applicable one-dimensional in-

The mass and stiffness matrices are as usual given by [5]

$$\mathbf{M}=\sum_m \mathbf{M}^{(m)}=\sum_m \int_{V^{(m)}} \widetilde{\rho}\mathbf{H}^{(m)\mathrm{T}}\mathbf{H}^{(m)}\mathrm{d}V \tag{6}$$

and

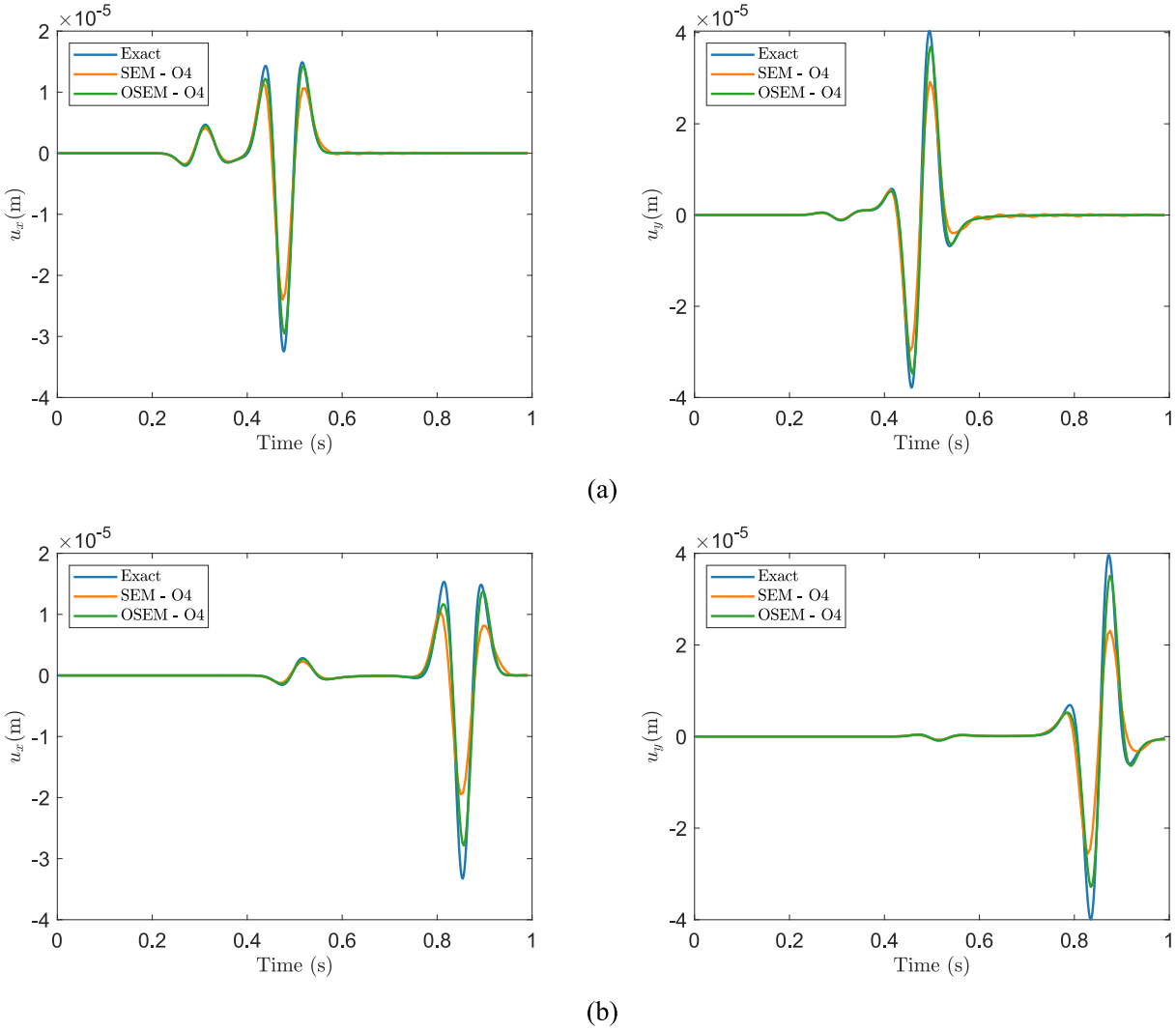

Fig. 8. Displacement histories obtained using overlapping spectral element method and spectral element method with a uniform mesh of 40 × 40 elements, compared to the analytical solution; Ricker wavelet loading: (a) horizontal (left) and vertical (right) displacements at $x = -640$ m, and (b) horizontal (left) and vertical (right) displacements at $x = -1280$ m.

$$\mathbf{K} = \sum_m \mathbf{K}^{(m)} = \sum_m \int_{V^{(m)}} \mathbf{B}^{(m)\mathrm{T}} \mathbf{C} \mathbf{B}^{(m)} \mathrm{d}V \tag{7}$$

in which $\widetilde{\rho}$, $\mathbf{C}$, and $\mathbf{B}$ denote the mass density, stress–strain law, and strain–displacement matrix. We note that since the GLL quadrature is used for the numerical integration, Eq. (6) gives a diagonal mass matrix considering the spectral interpolation functions.

2.2. Overlapping spectral element

An *overlapping* spectral element is an element with both traditional and additional degrees of freedom, thus expressing the unknown displacements in the element domain in terms of a polynomial basis at each node. For a linear basis we use, as for the overlapping finite elements [14],

$$u_K = a_{K1} + a_{K2}\frac{(x - x_K)}{d_K} + a_{K3}\frac{(y - y_K)}{d_K} + \ldots \tag{8}$$

in which a_{Ki} ($i = 1, 2, 3, \ldots, p$) are the unknown coefficients of node K, and d_K is equal to $\max_{J \in \Xi} \|\mathbf{x}_J - \mathbf{x}_K\|/2$ where Ξ denotes the set of nodes that are contained in the overlapping polygonal element of node K. However, the average element size can simply be used to define d_K and the results hardly change.

The coordinates of node K are defined as $\mathbf{x}_K = x_K$, $\mathbf{x}_K = (x_K, y_K)$, and $\mathbf{x}_K = (x_K, y_K, z_K)$ for a one-, two- and three-dimensional analysis, respectively. It should be noted that the traditional degree of freedom of node K corresponds to a_{Ki} with $i = 1$, and the additional degrees of freedom of that node correspond to a_{Ki} with $i > 1$. This statement implies that the former total number of unknowns (the traditional degrees of freedom) is multiplied by 3 for a two-dimensional overlapping element when using a linear basis. In general, the total number of unknowns for an overlapping element is equal to $p \times n$ where n is the number of traditional degrees of freedom. Thus, in Eq. (4), the matrix $\mathbf{H}^{(m)}$ and vector $\mathbf{a}^{(m)}$ of the overlapping spectral element can be written in terms of block matrices

$$\mathbf{h}_K = \rho_K \mathbf{p}_K \tag{9}$$

with

$$\mathbf{p}_K = \begin{bmatrix} 1 & \dfrac{(x - x_K)}{d_K} & \dfrac{(y - y_K)}{d_K} & \ldots \end{bmatrix}_{1 \times p} \tag{10}$$

Also, in a two-dimensional analysis we have for each node

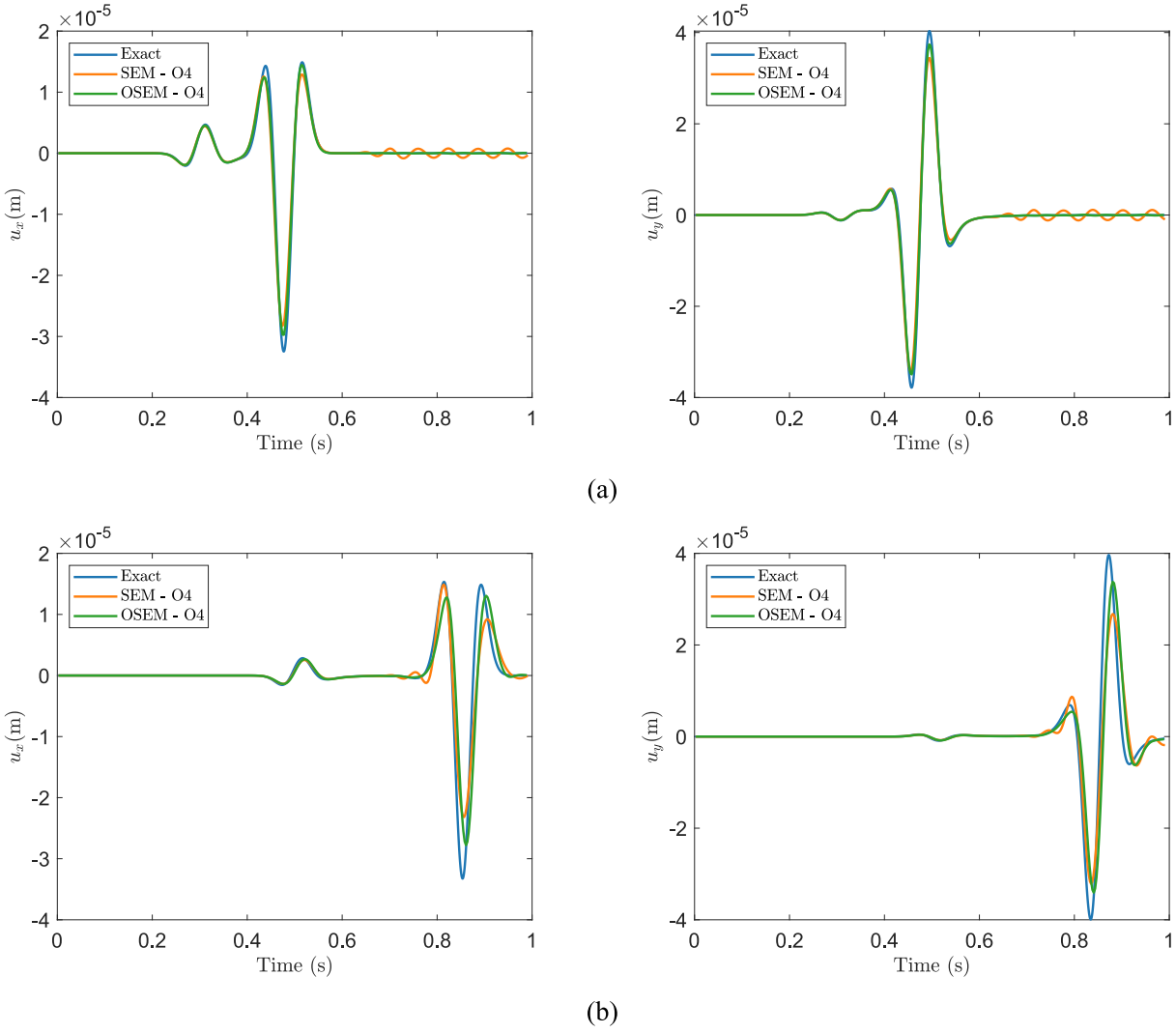

Fig. 9. Displacement histories obtained using overlapping spectral element method and spectral element method with a distorted mesh of 1936 elements, compared to the analytical solution; Ricker wavelet loading: (a) horizontal (left) and vertical (right) displacements at $x = -640$ m, and (b) horizontal (left) and vertical (right) displacements at $x = -1280$ m.

$$\begin{aligned}\mathbf{a}_K^u &= \left[a_{K1}^u \;\; a_{K2}^u \;\; a_{K3}^u \;\; \cdots \;\; a_{Kp}^u\right],\\ \mathbf{a}_K^v &= \left[a_{K1}^v \;\; a_{K2}^v \;\; a_{K3}^v \;\; \cdots \;\; a_{Kp}^v\right]\end{aligned} \tag{11}$$

where u and v stand for the two orthogonal directions.

In order to obtain the interpolation functions of an overlapping spectral element, the interpolation functions (h_i) of a low-order spectral element and a higher-order "fictitious" spectral element ($\widehat{h}_i$) can be used. The higher-order element is called "fictitious", because it is not a "real" spectral element considering the nodal positions. However, to reduce the computational cost the same-order element can also be utilized, instead of a higher-order spectral element, and we proceed that way. As shown in Fig. 1, we simply place the fictitious interior nodes at the mid-points between the two adjacent nodes near the corners of the low-order element, and proceed similarly for the two-dimensional element, see Fig. 2.

We use this approach because of the uneven spacing of the nodes in a spectral element and for this reason we also use the basic formulation given in Ref. [6]. Hence, the interpolation functions of an overlapping element are obtained using [6]

$$\phi_K^I = \sum_{i=1}^{M} \widehat{h}_i \widehat{\phi}_{Ki}^I \tag{12}$$

where I and K denote the nodes of the overlapping element that participate in the weighting coefficient ϕ_K^I, while M represents the total number of nodes in the fictitious same- or higher-order element; also, $\widehat{\phi}_{Ki}^I$ is the nodal value of the Shepard weight function at node i. As an example, in Fig. 2, we have $I, K = 1, 2, \ldots, 25$ and the use of the fictitious 4th-order element results in $M = 25$. This relation can also be written in matrix form

$$\boldsymbol{\varphi}_K = \widehat{\boldsymbol{\varphi}}_K \widehat{\mathbf{h}}^{\mathrm{T}} \tag{13}$$

where $\widehat{\mathbf{h}}$ is a row vector containing the interpolation functions of the fictitious same- or higher-order element, $\widehat{\boldsymbol{\varphi}}_K$ is a matrix containing the $\widehat{\phi}_{Ki}^I$ corresponding to an entry located at the Ith row and the ith column; and $\boldsymbol{\varphi}_K$ denotes a column vector including ϕ_K^I corresponding to the Ith row.

Then the interpolation functions used in Eq. (9) are

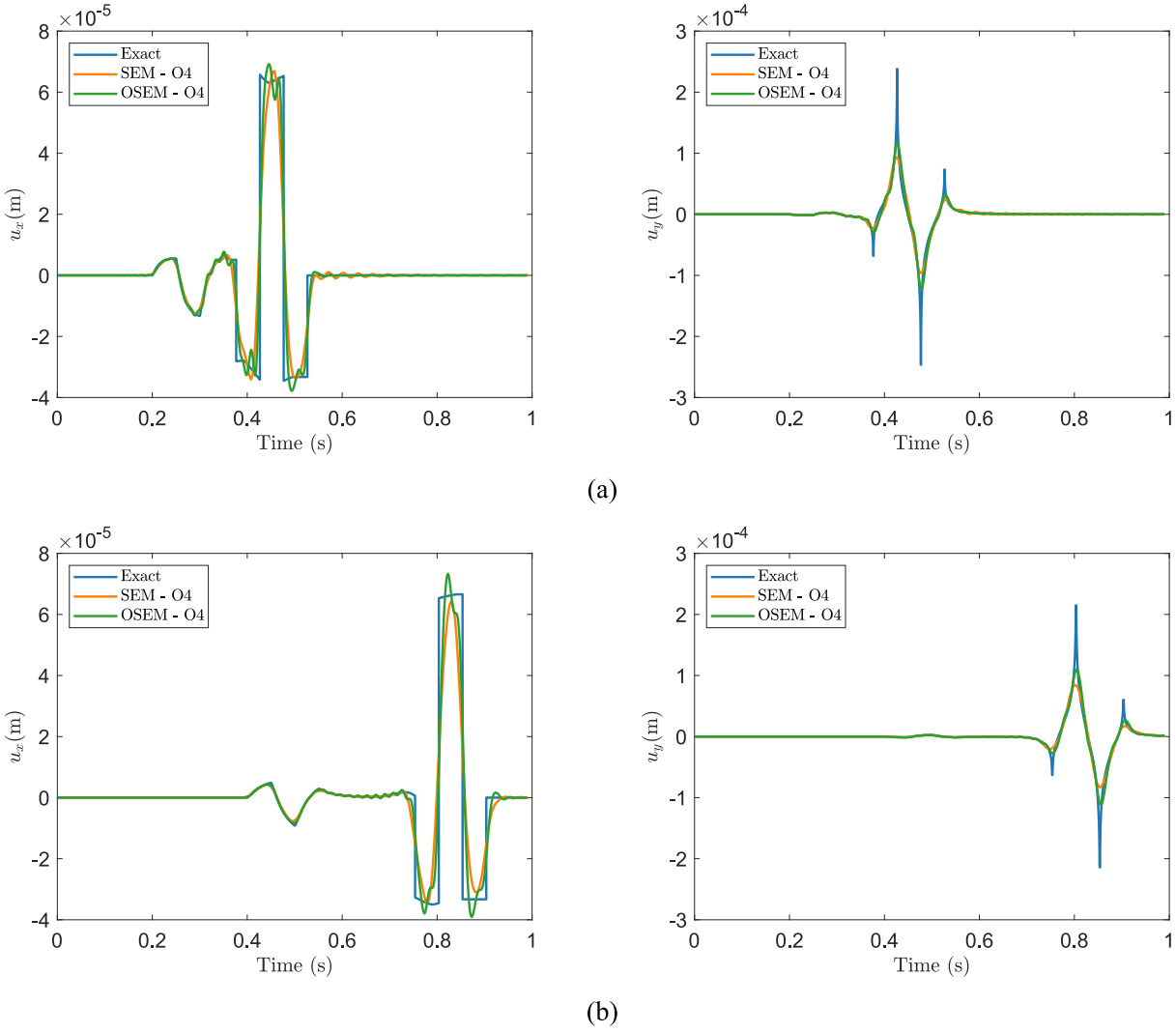

Fig. 10. Displacement histories obtained using the overlapping spectral element method and the spectral element method with a uniform mesh of 60 × 60 elements, compared to the analytical solution; step functions loading: (a) horizontal (left) and vertical (right) displacements at $x = -640$ m, and (b) horizontal (left) and vertical (right) displacements at $x = -1280$ m.

$$\rho_K = \sum_{l=1}^{N} h_l \phi_K^l \tag{14}$$

where N represents the total number of nodes for the overlapping element. Alternatively, Eq. (14) can be expressed in matrix form, as follows:

$$\rho_K = \mathbf{h}\boldsymbol{\varphi}_K \tag{15}$$

in which $\mathbf{h}$ is a row vector of the interpolation functions of the low-order traditional spectral element.

A constant parameter γ is used to establish the $\widehat{\phi}_{Ki}^I$, such that

$$\widehat{\phi}_{Ki}^I = \frac{W_K^I}{\sum_{J\in\Upsilon} W_J^I} \quad \text{with} \quad W_J^I = \begin{cases} \gamma h_J(x_i), & \text{for } I = J \\ h_J(x_i), & \text{for } I \neq J \end{cases} \tag{16}$$

in which Υ is the set of nodes of the low-order element, and we use $\gamma = 1.1$.

After determining the interpolation functions using Eq. (9), Eqs. (6) and (7) can be utilized to form the mass and stiffness matrices of overlapping spectral elements.

2.3. Coupling spectral element

As mentioned earlier, a *coupling* spectral element connects a regular spectral element to an overlapping spectral element in a mesh. Hence, nodes of the coupling spectral element are categorized into two groups: the first group includes the nodes intersected with the traditional spectral element, while the second group includes the nodes intersected with the overlapping spectral elements. The nodes in the first group have only the traditional degrees of freedom, whereas the nodes in the second group have both traditional and additional degrees of freedom. Accordingly, matrix $\mathbf{H}^{(m)}$ for a coupling element can be partitioned into two block matrices as $\mathbf{H}^{(m)} = [\mathbf{H}_{\text{SN}},\ \mathbf{H}_{\text{ON}}]$ wherein "SN" denotes the set of spectral-element nodes, and "ON" stands for the set of overlapping-spectral-element nodes.

The interpolation functions utilized in $\mathbf{H}_{\text{ON}}$ is computed by

$$\mathbf{h}_K^{\text{ON}} = \rho_K^{\text{SN}} \mathbf{p}_0 + \rho_K^{\text{ON}} \mathbf{p}_K \tag{17}$$

where

$$\rho_K^{\text{SN}} = \mathbf{h}\boldsymbol{\varphi}_K^{\text{SN}}, \quad \boldsymbol{\varphi}_K^{\text{SN},I} = \begin{cases} h_K & \text{for } I \in \text{SN} \\ h_K \sum_{j\in\text{SN}} \phi_j^I & \text{for } I \in \text{ON} \end{cases} \tag{18}$$

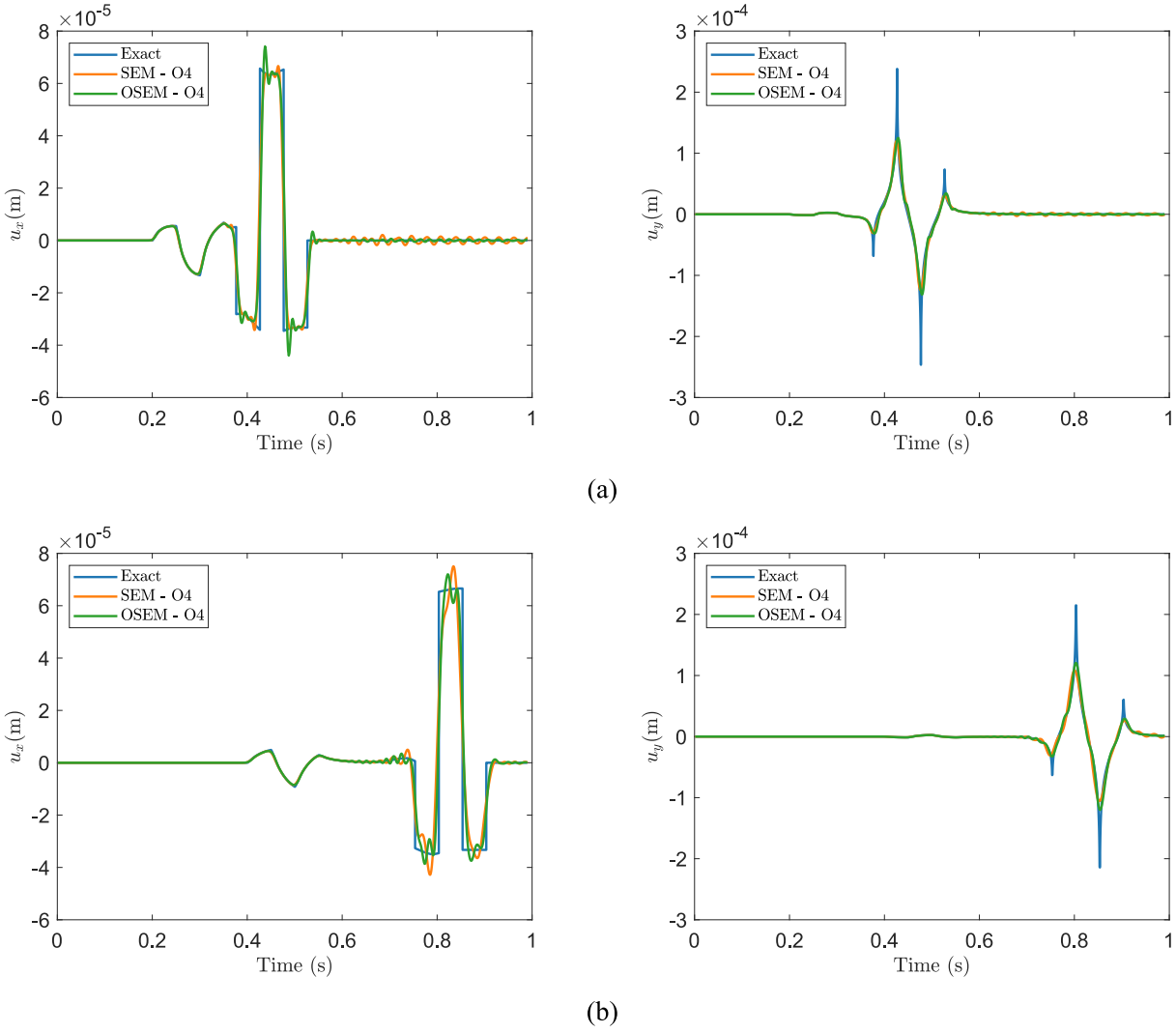

Fig. 11. Displacement histories obtained using the overlapping spectral element method and the spectral element method with a distorted mesh of 8100 elements, compared to the analytical solution; step functions loading: (a) horizontal (left) and vertical (right) displacements at $x = -640$ m, and (b) horizontal (left) and vertical (right) displacements at $x = -1280$ m.

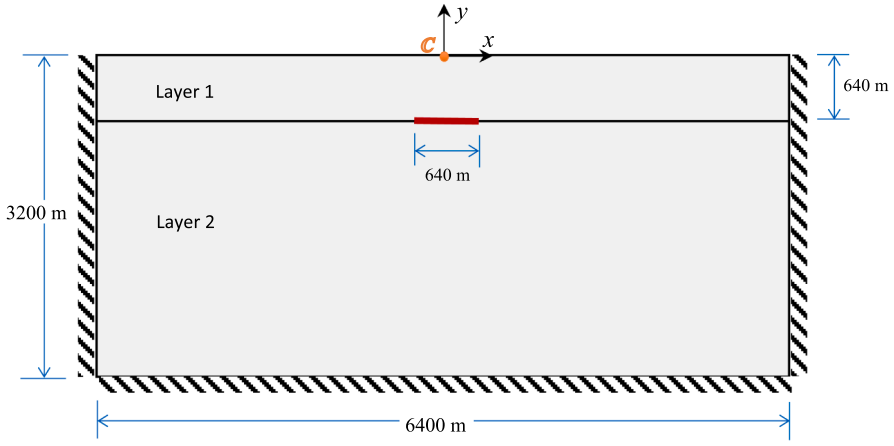

Fig. 12. Computational domain defined for wave propagation within double-layer semi-infinite elastic medium with an interface crack, where the excitation force is applied at point C and two receivers are located at $(-640$ m, 0) and $(-1280$ m, 0).

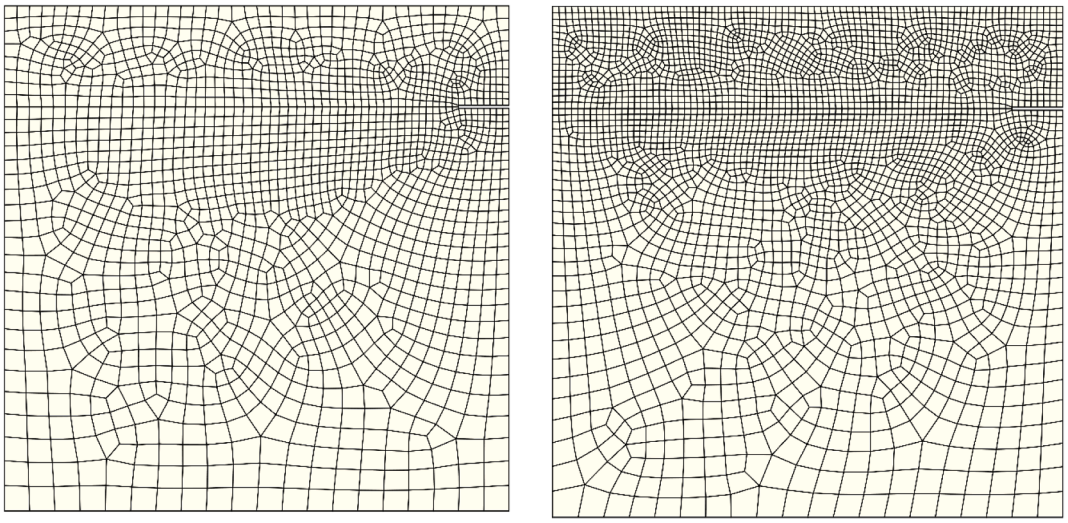

Fig. 13. Meshes used for the double-layer medium with an interface crack: (a) mesh of 1783 elements which is utilized when applying the Ricker wavelet loading, and (b) mesh of 3318 elements which is utilized when applying the series of step functions.

and

$$\rho_K^{\mathrm{ON}} = \mathbf{h}\boldsymbol{\varphi}_K^{\mathrm{ON}}, \quad \boldsymbol{\varphi}_K^{\mathrm{ON},I} = \begin{cases} 0 & \text{for } I \in \mathrm{SN} \\ \phi_K^I & \text{for } I \in \mathrm{ON} \end{cases} \tag{19}$$

such that $\boldsymbol{\varphi}_K^{\mathrm{SN},I}$ implies the Ith entry of the column vector $\boldsymbol{\varphi}_K^{\mathrm{SN}}$, and similarly $\boldsymbol{\varphi}_K^{\mathrm{ON},I}$ implies the Ith entry of the column vector $\boldsymbol{\varphi}_K^{\mathrm{ON}}$. As deduced from Eqs. (18) and (19), Eq. (15) cannot be utilized for the coupling spectral element.

On the other hand, using Eq. (18), the interpolation functions utilized in $\mathbf{H}_{\mathrm{SN}}$ is computed by

$$\mathbf{h}_K^{\mathrm{SN}} = \rho_K^{\mathrm{SN}} \tag{20}$$

Finally, displacements for the mth coupling spectral element are obtained by

$$\mathbf{U}^{(m)} = \mathbf{H}^{(m)}\mathbf{a}^{(m)} = [\mathbf{H}_{\mathrm{SN}},\ \mathbf{H}_{\mathrm{ON}}]\begin{bmatrix}\mathbf{a}_{\mathrm{SN}} \\ \mathbf{a}_{\mathrm{ON}}\end{bmatrix} \tag{21}$$

One can take $\mathbf{p}_K$ as in Eq. (10) and $\mathbf{p}_0$ as $\begin{bmatrix}1 & \overbrace{0 \quad \cdots \quad 0}^{p-1}\end{bmatrix}$. Also, the unknowns for each node like K in the set of "ON" are represented by

$$\begin{aligned}\mathbf{a}_K^u &= \begin{bmatrix}a_{K1}^u & a_{K2}^u & a_{K3}^u & \cdots & a_{Kp}^u\end{bmatrix}, \\ \mathbf{a}_K^v &= \begin{bmatrix}a_{K1}^v & a_{K2}^v & a_{K3}^v & \cdots & a_{Kp}^v\end{bmatrix}\end{aligned} \tag{22}$$

while the unknowns for such a node in the set of "SN" are indicated by

$$\begin{aligned}\mathbf{a}_K^u &= a_{K1}^u \\ \mathbf{a}_K^v &= a_{K2}^v\end{aligned} \tag{23}$$

It is worth mentioning that Eq. (20) and (23) give scalar values. Once again, after obtaining the interpolation functions with Eqs. (17) and (20) to form $\mathbf{H}^{(m)} = [\mathbf{H}_{\mathrm{SN}},\ \mathbf{H}_{\mathrm{ON}}]$, the mass and stiffness matrices of coupling spectral elements are established utilizing Eqs. (6) and (7).

3. Overlapping spectral interpolation functions

In this section, we derive the interpolation functions for bar and quadrilateral overlapping spectral elements shown in Figs. 1 and 2 with further details following Section 2.2.

3.1. A bar overlapping spectral element of order 3

A one-dimensional overlapping element of order 3 is shown in Fig. 1c, which is constructed with a 3rd-order spectral element and a fictitious 3rd-order spectral element as the low-order and same-order elements, respectively. The interpolation functions of the low-order element are listed as follows:

$$\begin{aligned} h_1 &= \frac{1}{8}\left(-5r^3+5r^2+r-1\right), \\ h_2 &= \frac{1}{8}\left(5\sqrt{5}\,r^3-5r^2-5\sqrt{5}\,r+5\right), \\ h_3 &= \frac{1}{8}\left(-5\sqrt{5}\,r^3-5r^2+5\sqrt{5}\,r+5\right), \\ h_4 &= \frac{1}{8}\left(5r^3+5r^2-r-1\right), \end{aligned} \tag{24}$$

which can also be obtained by substituting $s=-1$ into the first four interpolation functions given in Eq. (5). These interpolation functions (h_i) are utilized to establish $\mathbf{h}$. The nodal coordinates of this element are $r=\pm 0.4472$ and $r=\pm 1.0000$. Also, the nodal coordinates of the fictitious same-order element are $r=\pm 0.7236$ and $r=\pm 1.0000$, where $r=\pm 0.7236$ is calculated by averaging $r=\pm 0.4472$ and $r=\pm 1.0000$. Using these points and the Lagrange interpolants, the $\widehat{h}_i$ are obtained to form $\widehat{\mathbf{h}}$. Then, substituting the $\mathbf{h}$ and $\widehat{\mathbf{h}}$ into Eqs. (13) and (15) gives ρ_K.

Hence, the interpolation function matrix of this element takes the form

$$\mathbf{H}^{(m)} = [\mathbf{h}_1\ \mathbf{h}_2\ \mathbf{h}_3\ \mathbf{h}_4] = [\rho_1\mathbf{p}_1\ \rho_2\mathbf{p}_2\ \rho_3\mathbf{p}_3\ \rho_4\mathbf{p}_4] \tag{25}$$

where

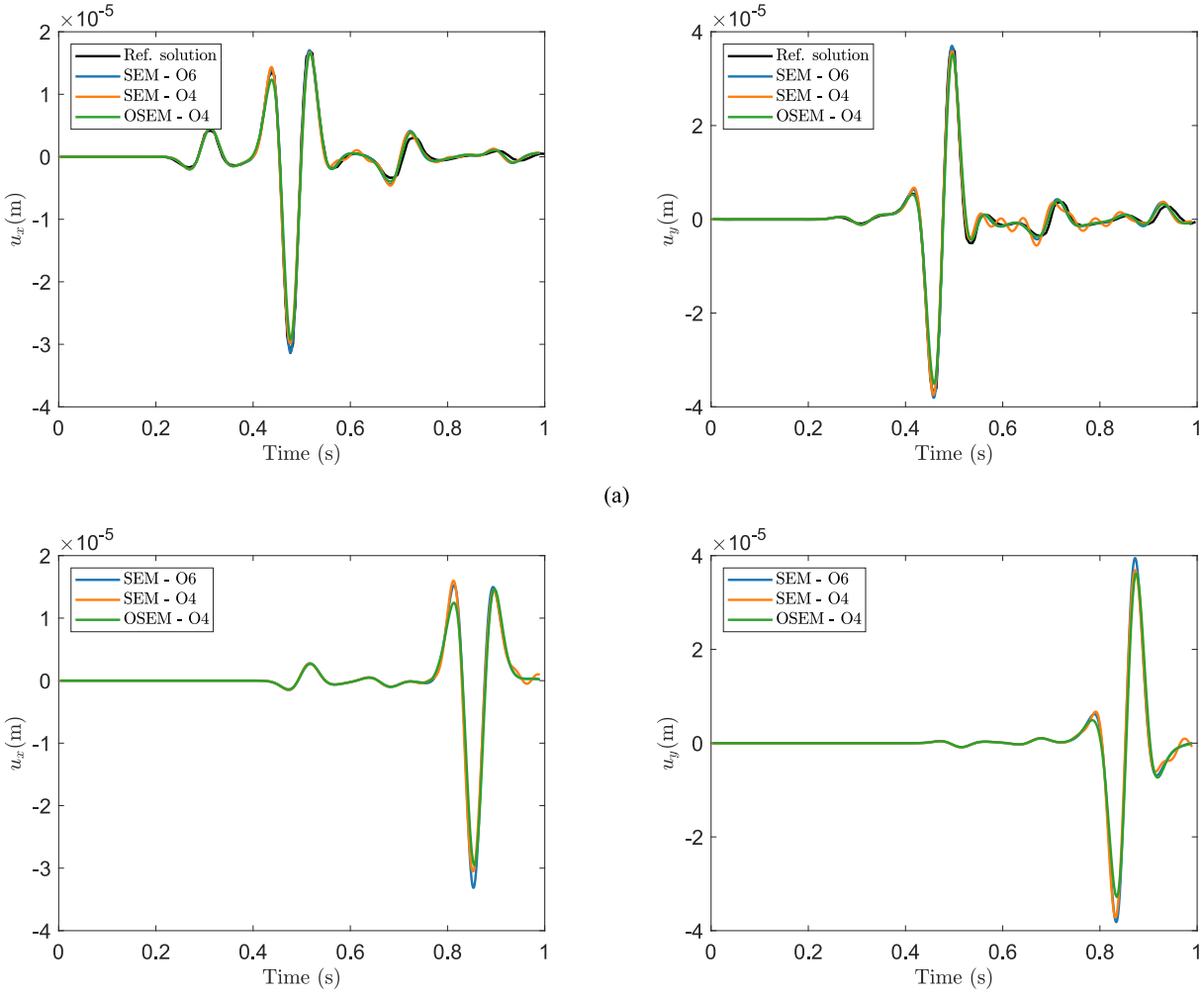

Fig. 14. Displacement histories obtained using overlapping spectral element method and spectral element method with a mesh of 1783 elements; Ricker wavelet loading: (a) horizontal (left) and vertical (right) displacements at x = −640 m—with a reference solution extracted from [8] that uses 23,608 overlapping finite elements, and (b) horizontal (left) and vertical (right) displacements at x = −1280 m.

$$\mathbf{p}_K = \left[1 \quad \frac{\left(\sum_{i=1}^{4} h_i x_i - x_K\right)}{d_K}\right], \quad K = 1,\ 2,\ 3,\ 4 \tag{26}$$

when using a linear polynomial basis. Also, the vector of unknowns is represented by

$$\mathbf{a}^{(m)} = \left[\mathbf{a}_1^u\ \mathbf{a}_2^u\ \mathbf{a}_3^u\ \mathbf{a}_4^u\right]^{\mathrm{T}} \tag{27}$$

with

$$\mathbf{a}_K^u = \left[a_{K1}^u\ a_{K2}^u\right], \quad K = 1,\ 2,\ 3,\ 4 \tag{28}$$

3.2. A quadrilateral overlapping spectral element of order 4

A two-dimensional overlapping element of order 4 is shown in Fig. 2c, which is established according to a 4th-order spectral element and a fictitious 4th-order spectral element as the low-order and same-order elements, respectively. According to Eq. (15), the interpolation functions are determined, where the nodal coordinates of the low-order element are ordered pairs (r, s) chosen from the combination of sets such that $r \in \{\pm 1.0000,\ \pm 0.6547,\ 0\}$ and $s \in \{\pm 1.0000,\ \pm 0.6547,\ 0\}$, while those of the same-order element are selected from the combination of sets such that $r \in \{\pm 1.0000,\ \pm 0.8273,\ 0\}$ and $s \in \{\pm 1.0000,\ \pm 0.8273,\ 0\}$. Nevertheless, the interpolation functions of the low-order element (h_i) and same-order elements ($\widehat{h}_i$) are not reported here for briefness, but they can be obtained similar to the procedure discussed in Section 3.1.

For the case where each node has two traditional degrees of freedom (as used in a plane-stress analysis), the interpolation function matrix of element takes the form

$$\mathbf{H}^{(m)} = \begin{bmatrix} \mathbf{h}_1 & \mathbf{0} & \mathbf{h}_2 & \mathbf{0} & \cdots & \mathbf{h}_{24} & \mathbf{0} & \mathbf{h}_{25} & \mathbf{0} \\ \mathbf{0} & \mathbf{h}_1 & \mathbf{0} & \mathbf{h}_2 & \cdots & \mathbf{0} & \mathbf{h}_{24} & \mathbf{0} & \mathbf{h}_{25} \end{bmatrix}$$
$$= \begin{bmatrix} \rho_1\mathbf{p}_1 & \mathbf{0} & \rho_2\mathbf{p}_2 & \mathbf{0} & \cdots & \rho_{24}\mathbf{p}_{24} & \mathbf{0} & \rho_{25}\mathbf{p}_{25} & \mathbf{0} \\ \mathbf{0} & \rho_1\mathbf{p}_1 & \mathbf{0} & \rho_2\mathbf{p}_2 & \cdots & \mathbf{0} & \rho_{24}\mathbf{p}_{24} & \mathbf{0} & \rho_{25}\mathbf{p}_{25} \end{bmatrix} \tag{29}$$

where

$$\mathbf{p}_K = \left[1 \quad \frac{\left(\sum_{i=1}^{25} h_i x_i - x_K\right)}{d_K} \quad \frac{\left(\sum_{i=1}^{25} h_i y_i - y_K\right)}{d_K}\right], \quad K = 1,\ 2,\ \cdots,\ 25 \tag{30}$$

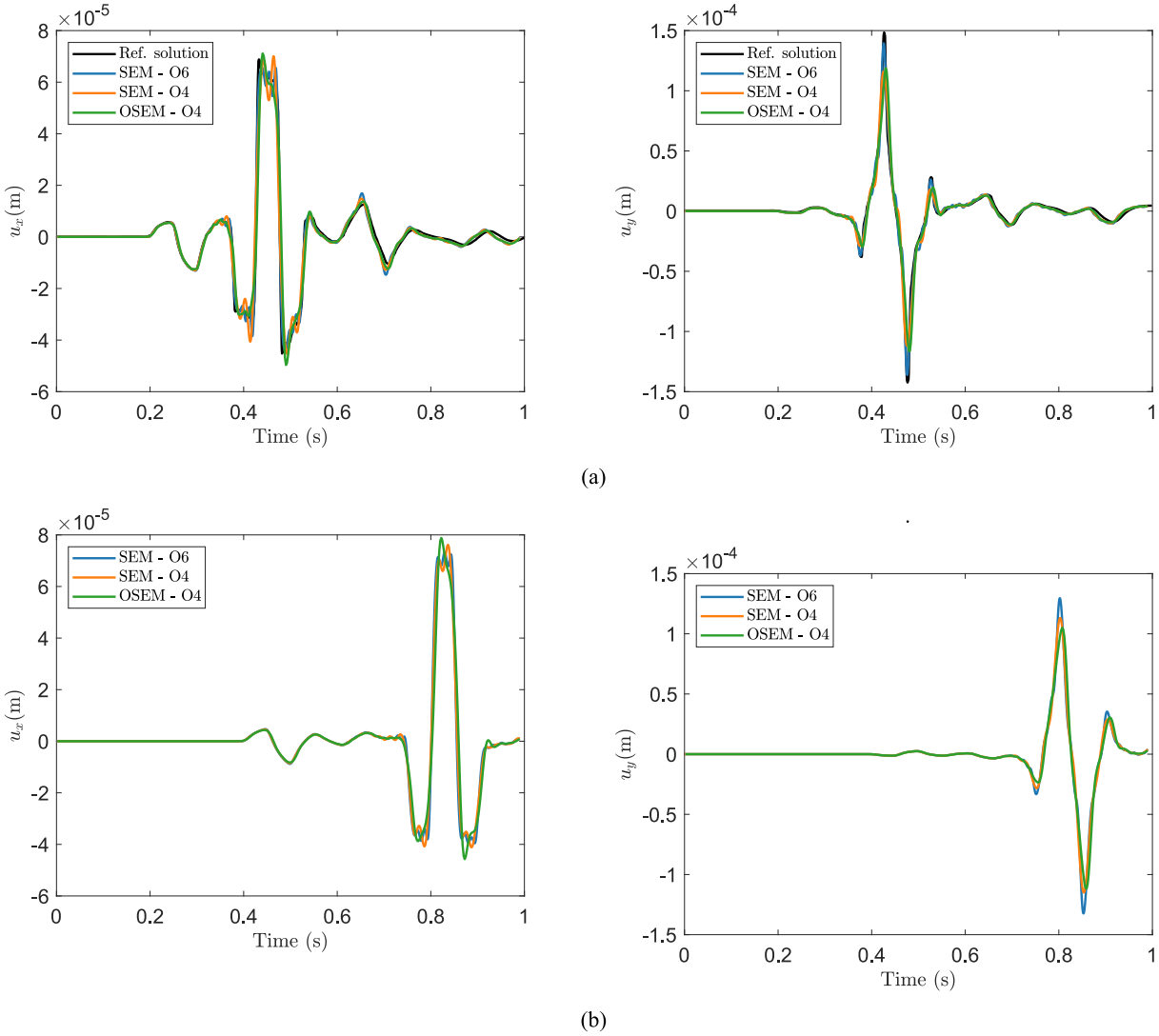

Fig. 15. Displacement histories obtained using the overlapping spectral element method and the spectral element method with a mesh of 3318 elements; step functions loading: (a) horizontal (left) and vertical (right) displacements at x = −640 m—with a reference solution extracted from [8] that uses 144,336 overlapping finite elements, and (b) horizontal (left) and vertical (right) displacements at x = −1280 m.

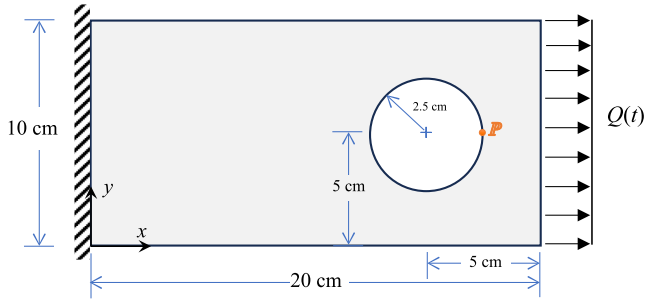

Fig. 16. An infinite strip with a circular hole subjected to harmonic loading; the strip is modeled as a two-dimensional problem in plane strain conditions.

when using a linear polynomial basis. Of course, in order to increase the computational efficiency of the GLL integration, the interpolation functions of 4-node finite element can be used in Eq. (30) to transform the x and y from the local to natural coordinate systems, considering $x = \sum_{i=1}^{4} h_i x_i$ and $y = \sum_{i=1}^{4} h_i y_i$. However, since the element edges usually are not curved, the spectral interpolation functions can also be employed with the same number of integration points, as applied to Eq. (30).

The vector of unknowns is

$$\mathbf{a}^{(m)} = [\mathbf{a}_1^u \quad \mathbf{a}_1^v \quad \mathbf{a}_2^u \quad \mathbf{a}_2^v \quad \cdots \quad \mathbf{a}_{24}^u \quad \mathbf{a}_{24}^v \quad \mathbf{a}_{25}^u \quad \mathbf{a}_{25}^v]^{\mathrm{T}} \tag{31}$$

with

$$\begin{aligned} \mathbf{a}_K^u &= [a_{K1}^u \ a_{K2}^u \ a_{K3}^u], \quad K = 1,\ 2,\ \cdots,\ 25 \\ \mathbf{a}_K^v &= [a_{K1}^v \ a_{K2}^v \ a_{K3}^v] \end{aligned} \tag{32}$$

For the case where each node has one traditional degree of freedom (as

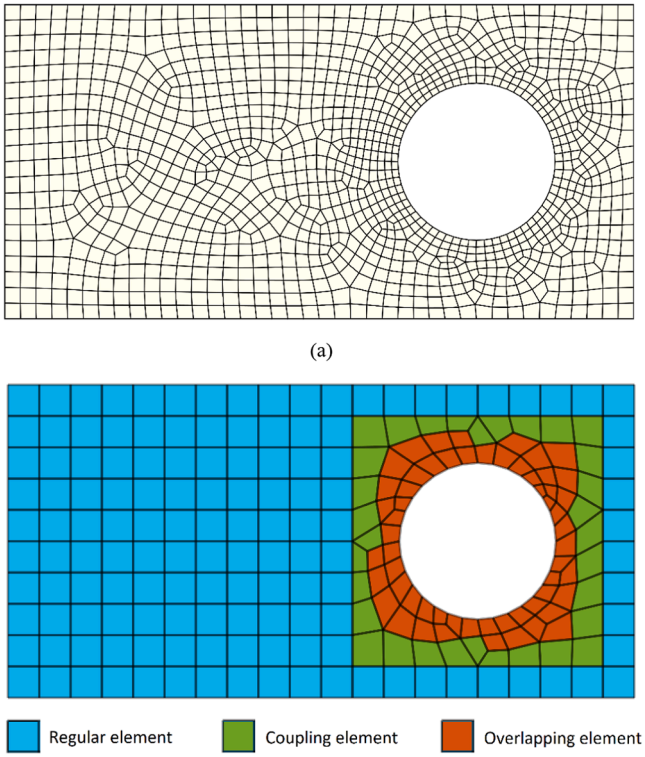

Fig. 17. Meshes used for the infinite strip with a circular hole: (a) a mesh of 1227 SEM elements, and (b) an AMORE mesh of 226 elements.

Table 1
Computational times (s) for the analyses of the infinite strip with a circular hole under harmonic loading.

Spectral element method	Overlapping spectral element method
1227 elements of order 6,with the explicit Bathe time integration	226 elements of order 4, with the explicit–implicit Bathe time integration
7.2969e+03	3.2839e+03

used in a scalar wave propagation problem), the interpolation function matrix of an element is expressed as

$$\mathbf{H}^{(m)} = [\,\mathbf{h}_1 \quad \mathbf{h}_2 \quad \cdots \quad \mathbf{h}_{24} \quad \mathbf{h}_{25}\,] = [\,\rho_1\mathbf{p}_1 \quad \rho_2\mathbf{p}_2 \quad \cdots \quad \rho_{24}\mathbf{p}_{24} \quad \rho_{25}\mathbf{p}_{25}\,] \tag{33}$$

for which the vector of unknowns is equal to

$$\mathbf{a}^{(m)} = [\,\mathbf{a}_1^u \quad \mathbf{a}_2^u \quad \cdots \quad \mathbf{a}_{24}^u \quad \mathbf{a}_{25}^u\,]^{\mathrm{T}} \tag{34}$$

with

$$\mathbf{a}_K^u = \left[a_{K1}^u \;\; a_{K2}^u \;\; a_{K3}^u\right], \quad K = 1,\ 2,\ \cdots,\ 25 \tag{35}$$

4. Numerical examples

In this section, the overlapping spectral element method is examined by several numerical experiments in order to demonstrate its abilities. According to the relevant literature [10,12,13,17], a spectral element with an order equal to or higher than 3 performs well for wave propagation problems. Therefore, here both 3rd-order and 4th-order overlapping spectral elements are utilized for the solution of the one-dimensional problem, whereas the 4th-order overlapping spectral element is employed for the solution of the two-dimensional problems. Both eigenvalue analyses and time-history dynamic analyses are carried out using the overlapping spectral element method (OSEM) and the spectral element method (SEM).

For explicit time integration, the β_1/β_2−Bathe scheme is utilized [18], while for implicit time integration, the ρ_∞−Bathe scheme with parameters $q_0 = (1-\beta_1)/2$, $q_1 = q_0$ and $q_2 = \beta_1$ is used [15]. With these parameters, of course, the ρ_∞−Bathe implicit time integration reduces to the β_1/β_2−Bathe implicit time integration [19]. The explicit time integration is applied when using a mesh of spectral elements, as a consistent mass matrix being “diagonal“ is produced. The implicit time integration is applied when using a mesh of overlapping spectral elements, as a consistent mass matrix (which is not diagonal) is produced.

Also, a combination of the selected Bathe explicit and implicit time integration schemes (an explicit–implicit scheme) is employed when using an AMORE mesh, because a partially diagonal mass matrix is generated.

Since we did not perform an optimization of the solution schemes, we do not report solution times when a relatively large number of degrees of freedom have been used. But for the last problem solution, involving a small number of elements, we can give solution times, merely to give an indication.

4.1. Eigenvalue analysis of a clamped rod

As shown in Fig. 3, a rod with fixed-free boundary condition is considered, for which the closed-from solution of the ith natural circular frequency is given as [20]

$$\omega_i = \frac{\pi}{2L}(2i-1)\sqrt{\frac{E}{\tilde{\rho}}} \tag{36}$$

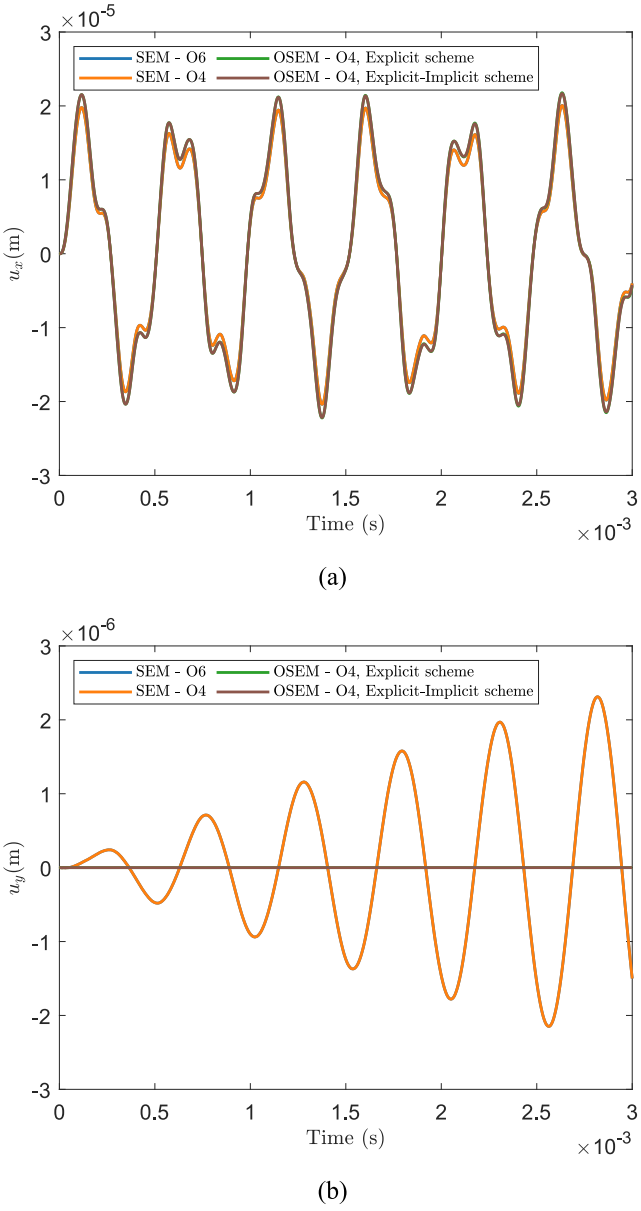

Fig. 18. Displacement histories at point P on the infinite strip with a circular hole obtained using overlapping spectral element method and spectral element method: (a) horizontal displacements, and (b) vertical displacements. In the figure, the blue and orange lines are almost identical, and the green and brown lines are also almost identical. (For interpretation of the references to colour in this figure legend, the reader is referred to the web version of this article.)

where $\widetilde{\rho}$, L, and E are the mass density, length, and elasticity modulus, respectively. The material and geometric properties of this structure are assumed to be $E = 200$ GPa, $\widetilde{\rho} = 7800$ kg/m^3, and $L = 5$ m, respectively.

The first ten natural frequencies of the structure are calculated with the analytical method, spectral element method, and overlapping spectral element method. Four elements are employed for the mesh of each numerical method. Since the highest polynomial degree in the interpolation functions of an overlapping spectral element is greater than that of the spectral element of the same order, more GLL points are required. For the integration of a polynomial with a degree up to $2q$-3, the GLL quadrature with q points is accurate. However, traditionally a reduced integration with $n + 1$ GLL points are employed for a spectral element of order n to render a diagonal mass matrix. Here, both stiffness and mass matrices use $n + 1$ GLL points. On the other hand, for an overlapping spectral element of order n, the stiffness and mass matrices employ $2n + 1$ and $2n + 2$ GLL points, respectively. Figs. 4a and 4b show the computed eigenvalues using overlapping spectral elements of order 3 and 4 for various numbers of GLL points, respectively. We give the number of GLL points employed in the calculation of the stiffness matrix, with one more GLL point added in the calculation of the mass matrix. Fig. 4 demonstrates that 7 and 9 GLL points are sufficient to accurately calculate the eigenvalues using the overlapping spectral elements of order 3 and 4, respectively.

As illustrated in Fig. 5, when using the appropriate number of GLL points for each element, even a 3rd-order overlapping spectral element can outperform both 3rd-order and 4th-order spectral elements in the accuracy of eigenvalues calculated.

4.2. *Wave propagation in a uniform semi-infinite medium*

Here, Lamb's problem is considered [8], which involves the propagation of P and SV waves in a semi-infinite isotropic elastic medium under plane strain conditions, as illustrated in Fig. 6. The medium is characterized by a mass density of $\widetilde{\rho} = 2200$ kg/m^3, elasticity modulus

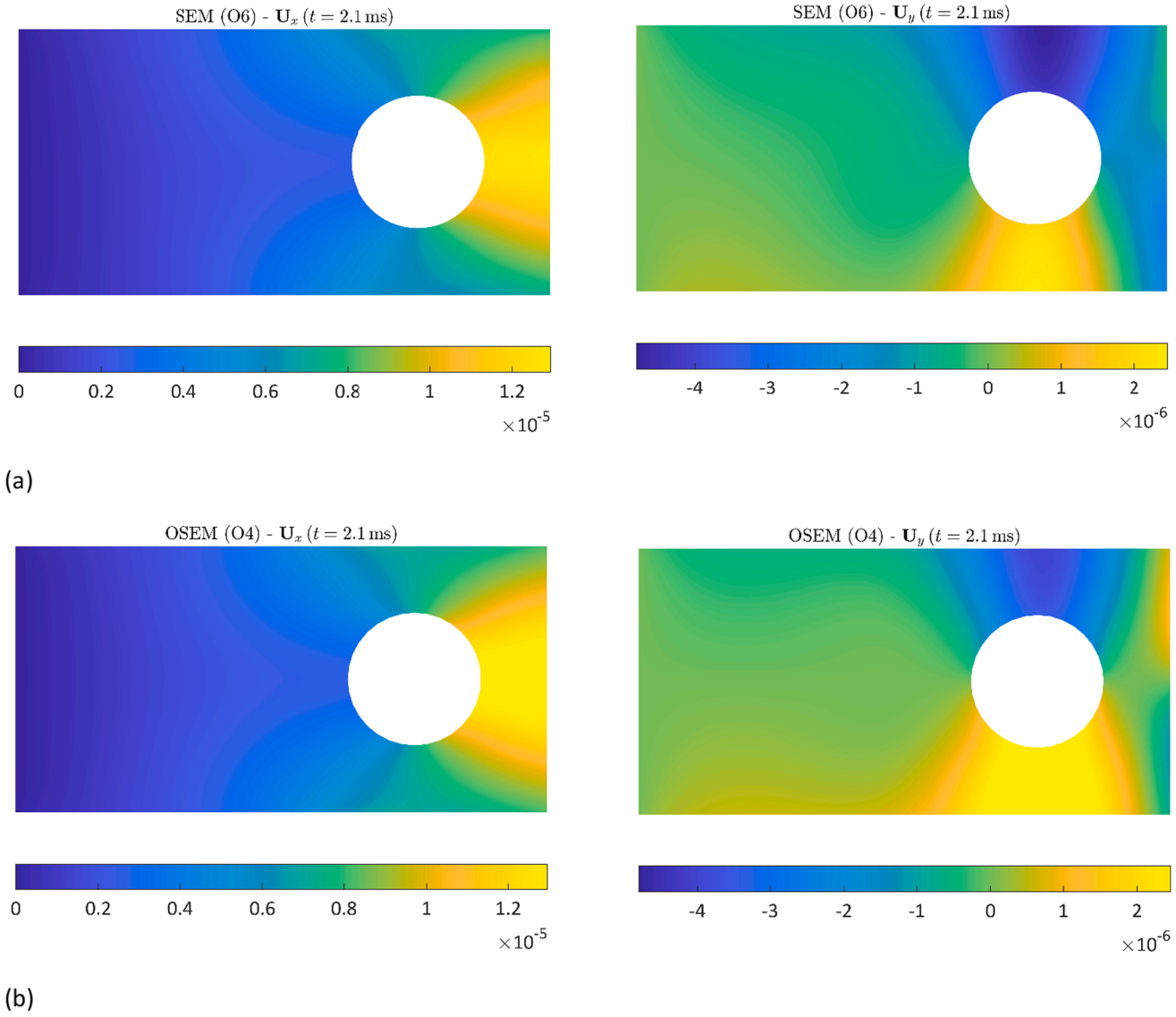

Fig. 19. Horizontal (left) and vertical (right) displacement fields of the infinite strip with a circular hole at $t = 2.1$ ms, obtained using: (a) spectral elements of 6th order, and (b) overlapping spectral elements of 4th order using the explicit–implicit Bathe time integration.

$E = 1.8773 \times 10^{10}$ N/m^2, and Poisson's ratio $\nu = 0.25$. These parameters result in a P-wave velocity $c_p = 3200$ m/s and an S-wave velocity $c_s = 1847.5$ m/s. Initially at rest, the medium is subjected to a concentrated line load applied at point C on the free surface. For the simulation, we use symmetry and define the computational domain as half of the total domain (see Fig. 7). Two types of excitations are considered: a Ricker wavelet loading and a loading of a series of step functions.

The spectral element method and overlapping spectral element method are employed to solve this problem, and the results are compared to those of the analytical method computed by Green's functions [21] and the convolution integral. For the implicit Bathe time integration applied to the overlapping spectral elements, the time step size (Δt) is determined based on the P-wave velocity using $CFL = v\Delta t/h_{eq} = 0.125$ and an equivalent element size of $h_{eq} = \sqrt{3200^2/N}$, where N is the total number of elements in the mesh (considering the symmetry) and v is the fastest wave velocity. For the explicit Bathe time integration applied to spectral elements, the time step size is taken as $\Delta t = 3.33/\omega_{\max}$, where $\omega_{\max}$ denotes the largest circular frequency of the computational domain.

The calculated displacements are recorded at the two receiver locations: $\mathbf{x} = (-640, 0)$ and $\mathbf{x} = (-1280, 0)$.

4.2.1. Ricker wavelet loading

The Ricker wavelet concentrated load applied upwardly at point C is given as

$$F(t) = A[1 - 2\pi^2 f_p^2 (t - t_s)^2]\, e^{-\pi^2 f_p^2 (t - t_s)^2} \tag{37}$$

with $A = 2 \times 10^6$, $f_p = 10$ Hz, and $t_s = 0.1$ s.

For solution, a uniform mesh of 40×40 elements and a distorted mesh of 1936 elements are utilized, as shown in Fig. 7. These meshes are used for both the spectral element analysis and the overlapping spectral element analysis. The displacement responses recorded at the two receivers are shown in Figs. 8 and 9. Compared to the analytical solutions, the results demonstrate that the overlapping spectral element method shows less distortion-sensitivity and higher accuracy than the spectral element method when using the same mesh.

4.2.2. Loading of a series of step functions

As the second excitation, a concentrated load consisting of three step functions is applied upwardly at point C, as defined by

$$F(t) = 2 \times 10^6 [H(0.15 - t) - 3H(0.1 - t) + 3H(0.05 - t)] \quad (38)$$

which requires fine meshes to achieve a sufficiently accurate solution because this discontinuous loading excites many frequencies, rendering the problem more challenging than when a Ricker wavelet is applied. The excitation of more modes implies that a larger number of modes contributes to the dynamic response.

For solution, a uniform mesh of 60 × 60 elements and a distorted mesh of 8100 elements are utilized, with configurations similar to those shown in Fig. 7. These meshes are used for both the spectral element analysis and the overlapping spectral element analysis. The displacement response recorded at the two receivers is given in Figs. 10 and 11 and shows some spurious oscillations.

Here we should note that a discontinuous function (like the applied load) is non-smooth and can impair the convergence of spectral elements [10].

4.3. Wave propagation in a double-layer medium with an interface crack

In this section, we address a wave propagation problem for which no analytical solution exists [8]. Consequently, we employ three numerical solutions for each simulation using spectral elements of order 6, spectral elements of order 4, and overlapping spectral elements of order 4. As illustrated in Fig. 12, this example involves the simulation of P and SV waves generated by a concentrated line force. These waves propagate through a semi-infinite elastic medium under plane strain conditions. The medium comprises two elastic layers and a small crack which provides a strong discontinuity. The first layer retains the same material properties as previously defined in Section 4.2, with a P-wave velocity of $c_{p_1} = 3200$ m/s and a S-wave velocity $c_{s_1} = 1847.5$ m/s, whereas the second layer features a reduced elasticity modulus, specifically $E_2 = 0.25E_1$, resulting in a P-wave velocity of $c_{p_2} = 1600$ and a S-wave velocity $c_{s_2} = 923.75$ m/s with Poisson's ratio and mass density being equal to those of the first layer. As seen in Fig. 12, the depth of the first layer and the length of the interfacial crack measure 640 m.

As in previous example, the excitation is modeled using a concentrated load applied to the free surface, represented either by a Ricker wavelet or a series of step functions. Considering symmetry, Fig. 13a shows the element mesh when applying the Ricker wavelet, whereas Fig. 13b illustrates the element mesh when applying the series of step functions. This example exclusively utilizes unstructured meshes, which are progressively refined toward the free surface and around the crack. Although the same mesh configuration is considered for each loading, obviously, element order or type is different when applied to spectral element and overlapping spectral element methods.

The time step sizes are selected as in Section 4.2, with the fastest wave velocity (P-wave velocity in layer 1) determining the CFL.

4.3.1. Ricker wavelet loading

We consider first the dynamic analysis when the Ricker wavelet loading defined by Eq. (37) is applied. The mesh shown in Fig. 13a is used for the spectral element analysis and the overlapping spectral element analysis to solve the problem, where we use 6th-order spectral elements, 4th-order spectral elements, and 4th-order overlapping spectral elements.

The displacement responses recorded at the two receivers are shown by Fig. 14. The results show that the overlapping spectral element solution is quite close to the 6th-order spectral element solution, while the 4th-order spectral element solution (with the same mesh) cannot achieve such an accuracy. We also observe that spurious oscillations are almost not present when using the overlapping spectral elements, which is not seen when using spectral elements of the same order.

4.3.2. Loading of a series of step functions

For the dynamic analyses when the loading of a series of step functions defined by Eq. (38) is applied, the mesh shown in Fig. 13b is used for both the spectral element analysis and overlapping spectral element analysis, using 6th-order spectral elements, 4th-order spectral elements, and 4th-order overlapping spectral elements.

Fig. 15 shows the displacement histories recorded at the receivers, which are consistent with the solutions given in Ref. [8]. The reference solution illustrated for $x = 640$ m in Fig. 15 (as in Fig. 14) is captured from Ref. [8] using an image-processing tool.

The results show some spurious oscillations and we note again, as in Section 4.2.2, that a discontinuous function (like the applied load) is non-smooth and can impair the convergence of spectral elements [10].

4.4. An infinite strip under harmonic loading

We consider an infinite strip with a circular hole subjected to a uniformly distributed harmonic loading [22], $Q(t) = 10\sin(4000\pi t)$ MPa, as shown in Fig. 16. The modulus of elasticity, Poisson's ratio, and mass density of this structure are taken as 200 GPa, 0.3, and 7800 kg/m^3, respectively.

As in the previous example, the spectral element method with an unstructured mesh illustrated in Fig. 17a is utilized using 1227 elements of 4th-order and 6th-order. We also use the overlapping spectral element method with the AMORE mesh comprising 226 elements of 4th-order, including regular, coupling, and overlapping elements (see Fig. 17b). Hence, the overlapping spectral element method employs a relatively coarse mesh, compared to the mesh used with the spectral element method. The explicit Bathe time integration scheme is employed when using the spectral element method, but both explicit and explicit–implicit Bathe time integration schemes are applied when using the overlapping spectral element method. For the explicit–implicit scheme, the critical time step size is calculated based on the explicit subdomain for which the mass matrix is diagonal, and hence it can be increased relative to the critical time step calculated based on the full domain (as calculated for the explicit scheme). Therefore, the use of explicit–implicit time integration reduces the computational cost in comparison to using only the explicit time integration (see Table 1).

For all analyses reported in the paper, we used a computer with the Intel Core i7-4790 K CPU @4.00 GHz with 24 GB RAM considering no optimization of the solution schemes. Hence while in general, when using many elements, the overlapping spectral element solutions may be expected to be computationally more expensive, valid solution times to compare can only be given when optimized solvers have been used. However, the number of degrees of freedom in the problem solution considered here is relatively small and we can report the solution times, just to give an indication of effectiveness.

The horizontal and vertical displacement histories at point P on the structure are shown in Fig. 18. Since point P is located on the axis of symmetry of both the structure and loading, the vertical displacement at that point for the continuum should be zero, and the values predicted in the overlapping spectral element solutions are very small (in the figure they overlap at the zero value), although a non-symmetric mesh is used. The spectral element solutions, on the other hand, also using a non-symmetric mesh, show a much larger vertical response. Furthermore, Fig. 19 gives the displacement fields at $t = 2.1$ ms and shows symmetry when using the overlapping spectral element method. According to Table 1 and Figs. 18 and 19 when using the explicit–implicit Bathe time integration, the overlapping spectral element method, using a relatively coarse mesh, can achieve the solution quality of a fine mesh of 6th-order spectral elements, while offering higher computational efficiency and accuracy.

5. Concluding remarks

In this paper, we developed the overlapping spectral element method as a new computational framework to simultaneously include advantages of both the spectral element method and the overlapping finite

element method. The proposed method is based on extending the higher-order interpolation functions of the spectral element method, while using the GLL quadrature.

Compared to using the spectral elements, the overlapping spectral elements are remarkably distortion-insensitive and provide higher solution accuracy. Hence although the spectral element method (with a diagonal mass matrix) is computationally more efficient than the overlapping spectral element method when using only overlapping elements (with a non-diagonal mass matrix), it is less accurate for the same mesh. It follows that, using the overlapping spectral elements, one can achieve higher accuracy with a mesh coarser than that used for the spectral elements. However, we only observed the significantly better accuracy provided the loading is smooth.

Furthermore, the computational efficiency of the proposed method is indicated when using an AMORE mesh, because the explicit–implicit time integration scheme can be used to provide high accuracy and lower computational cost. In the example given, the AMORE coarse mesh using overlapping spectral elements requires less solution time and gives more accurate results than the spectral element method with a finer mesh of even higher-order elements. This point is important because, for example, the overlapping spectral element of order 4 can provide better solution accuracy than that obtained using the spectral element of order 6.

In future research, it would of course be valuable to try to increase even further the accuracy and decrease the cost of the solution scheme and in addition it would also be valuable to look in more detail at how best the solution scheme can be optimized to reach the least computational cost. This requires, for example, to establish the most effective equation solvers regarding storage needed and solution times used, and, also, how best to perform the explicit–implicit Bathe time integration in the AMORE scheme.

CRediT authorship contribution statement

Pooya Zakian: Methodology, Investigation, Formal analysis. **Klaus-Jürgen Bathe:** Writing – review & editing, Methodology, Investigation, Conceptualization.

Declaration of competing interest

The authors declare that they have no known competing financial interests or personal relationships that could have appeared to influence the work reported in this paper.

Data availability

No data was used for the research described in the article.

References

[1] Hori M. Introduction to Computational Earthquake Engineering. 2nd ed. London: Imperial College Press; 2011.
[2] Igel H. Computational Seismology: a Practical Introduction. New York: Oxford University Press; 2017.
[3] Zakian P, Khaji N. A stochastic spectral finite element method for solution of faulting-induced wave propagation in materially random continua without explicitly modeled discontinuities. Comput Mech 2019;64:1017–48.
[4] Ostachowicz W, Kudela P, Krawczuk M, Zak A. Guided Waves in Structures for SHM: the Time - domain Spectral Element Method. Chichester: Wiley; 2012.
[5] Bathe KJ. Finite Element Procedures: Prentice Hall; 1996, 2nd edition, 2014 KJ Bathe, amazon.com, Springer Nature, in press; Finite Element Procedures — En Plus, Springer Nature, in press.
[6] Bathe KJ. The AMORE paradigm for finite element analysis. Adv Eng Softw 2019;130:1–13.
[7] Chai Y, Bathe KJ. Transient wave propagation in inhomogeneous media with enriched overlapping triangular elements. Comput Struct 2020;237:106273.
[8] Kim K-T, Bathe KJ. Accurate solution of wave propagation problems in elasticity. Comput Struct 2021;249:106502.
[9] Kim K-T, Zhang L, Bathe KJ. Transient implicit wave propagation dynamics with overlapping finite elements. Comput Struct 2018;199:18–33.
[10] Zakian P, Bathe KJ. Transient wave propagations with the Noh-Bathe scheme and the spectral element method. Comput Struct 2021;254:106531.
[11] Komatitsch D, Tromp J. Introduction to the spectral element method for three-dimensional seismic wave propagation. Geophys J Int 1999;139:806–22.
[12] Komatitsch D, Vilotte J-P, Vai R, Castillo-Covarrubias JM, Sánchez-Sesma FJ. The spectral element method for elastic wave equations—application to 2-D and 3-D seismic problems. Int J Numer Meth Eng 1999;45:1139–64.
[13] Galvez P, Ampuero JP, Dalguer LA, Somala SN, Nissen-Meyer T. Dynamic earthquake rupture modelled with an unstructured 3-D spectral element method applied to the 2011 M9 Tohoku earthquake. Geophys J Int 2014;198:1222–40.
[14] Lee S, Bathe KJ. An enhancement of overlapping finite elements. Comput Struct 2022;260:106704.
[15] Noh G, Bathe KJ. The Bathe time integration method with controllable spectral radius: the ρ∞-Bathe method. Comput Struct 2019;212:299–310.
[16] Zakian P, Khaji N. A novel stochastic-spectral finite element method for analysis of elastodynamic problems in the time domain. Meccanica 2016;51:893–920.
[17] Zakian P. Stochastic spectral cell method for structural dynamics and wave propagations. Int J Numer Meth Eng 2023;124:4769–801.
[18] Malakiyeh MM, Shojaee S, Hamzehei-Javaran S, Bathe KJ. The explicit β1/β2-Bathe time integration method. Comput Struct 2023;286:107092.
[19] Malakiyeh MM, Shojaee S, Bathe KJ. The Bathe time integration method revisited for prescribing desired numerical dissipation. Comput Struct 2019;212:289–98.
[20] Clough RW, Penzien J. Dynamics of Structures. 3rd ed: Computers and Structures Inc; 2003.
[21] Miklowitz J. The Theory of Elastic Waves and Waveguides. Amsterdam: Elsevier; 1978.
[22] Lee S, Bathe KJ. Solution of the generalized eigenvalue problem using overlapping finite elements. Adv Eng Softw 2022;173:103241.